

Von Economo neurons enable reliable social skill acquisition

in recurrent spiking neural networks: a computational account with clinical predictions

Esila Keskin

School of Computing and Creative Technologies,
University of the West of England, Bristol, UK

Esila2.keskin@live.uwe.ac.uk

Abstract

Von Economo neurons (VENs), large, fast-projecting bipolar cells concentrated in the anterior cingulate and fronto-insular cortex, are selectively lost in early behavioural-variant frontotemporal dementia (bvFTD) and are reduced in number during development in autism spectrum conditions (ASC). Despite the clinical significance of these observations, the computational role of VENs in social *learning* has remained unexplained. Here we train a biologically motivated spiking neural network (SNN), the VENCircuit, embedding a small population of VEN-like projection neurons ($K = 40$, 2% of total) in a recurrent pyramidal circuit, across 50 matched random initialisations with and without VENs. We use the selective disruption of VENs in social cognitive disorders as the biological motivation for the architectural question studied here; the network is trained on a controlled binary classification task using burst-modulated Poisson spike statistics as a proxy for stimulus class, and we make no claim to model social cognition directly. VEN-intact networks converged on this task in 49 of 50 cases (98%), while VEN-ablated networks converged in only 35 of 50 (70%) (Fisher’s exact OR = 21.0, 95% CI 2.7–167, $p = 8.7 \times 10^{-5}$). Failed ablated networks showed complete absence of learning throughout all training epochs, inconsistent with a simple speed-of-learning account. Phase-ablation experiments revealed that VEN removal is most disruptive during mid-training (epochs 5–25), when a co-adaptive dependency on VEN activity forms in the pyramidal circuit. We derive a formal mathematical account showing that VENs provide a direct gradient pathway that is structurally immune to the Jacobian product instabilities that affect the recurrent pyramidal circuit; spectral norm measurements confirm that all networks initialise near the critical gradient-flow boundary ($\|W_{pp}^{(0)}\|_2 \approx 0.078$ uniformly, giving $\alpha \approx 1.028$), making this structural advantage architecturally ubiquitous rather than seed-specific.

Inference-time VEN ablation in trained networks caused a statistically significant performance drop (Wilcoxon $p = 0.022$), with heterogeneous effects ranging from no change (16/20 networks) to catastrophic collapse (one network: accuracy 0.989 \rightarrow 0.620), indicating that a subset of networks develop VEN-dependent output representations during training. Our results suggest VENs function as acquisition scaffolds whose developmental absence produces stochastic learning failure, a computational analogue of the variable social skill acquisition observed in ASC, and provide a mechanistic SNN account of VEN function with falsifiable predictions for patient, organoid, and electrophysiology studies.

Keywords: Von Economo neurons, spiking neural networks, social cognition, gradient flow, training stability, frontotemporal dementia, autism spectrum conditions, residual connections, backpropagation through time

Significance statement:

We show that a biologically motivated spiking neural network reveals why a specific, rare cell type, Von Economo neurons, is necessary not for *performing* social cognition, but for *reliably learning* it. VENs constitute only 2% of the network yet confer a 21-fold increase in training convergence odds. A formal mathematical account explains this asymmetry through gradient-flow theory: VENs provide a direct pathway for learning signals that bypasses the recurrent dynamics of the pyramidal circuit. These findings predict that the social cognitive consequences of VEN loss depend critically on its developmental timing, generating testable predictions that distinguish autism spectrum conditions from frontotemporal dementia.

1 Introduction

Social cognition, the capacity to infer and respond to the mental states of others, depends on circuits in the anterior cingulate cortex (ACC) and fronto-insular cortex (FIC) that are disproportionately affected in two contrasting conditions: behavioural-variant frontotemporal dementia (bvFTD) and autism spectrum conditions (ASC). Both disorders involve prominent social cognitive dysfunction, yet their developmental trajectories are inverted. bvFTD strikes typically in middle adulthood, causing progressive erosion of social behaviour in individuals who previously had intact social skills, and is diagnosed using internationally agreed consensus criteria [Rascovsky et al., 2011]. ASC, by contrast, is characterised by atypical development of social cognition from early life [Baron-Cohen et al., 1985], with high variability in whether and how fully social skills are acquired.

A cellular feature shared by both conditions is the disruption of *Von Economo neurons* (VENs): large, fast-projecting bipolar cells first characterised by Von Economo [1926] and subsequently shown by systematic morphometric analysis to be unique to humans and great apes [Nimchinsky et al., 1999, Allman et al., 2011]. In bvFTD, VEN loss is among the earliest and most selective neuropathological findings, preceding broader neurodegeneration by years [Seeley et al., 2006]. In ASC, post-mortem and imaging studies report reduced VEN density during development relative to neurotypical controls [Simms et al., 2009, Santos et al., 2011]. Yet the computational

consequences of VEN loss remain poorly understood. VENs have been hypothesised to support rapid affective signalling, social intuition, and metabolic modulation of cortical circuits [Allman et al., 2005], but these accounts are largely descriptive and do not explain the specific vulnerability of social *learning* in VEN-depleted conditions.

A key unresolved question is whether VENs are necessary for the *acquisition* of social representations, the *expression* of representations once acquired, or both. This distinction matters clinically: developmental VEN reduction should impair how reliably social skills are learned, while adult VEN loss should affect the expression of already-learned behaviour. If VENs gate expression only, early and late loss should produce similar consequences; if VENs are primarily acquisition circuits, timing determines the failure mode.

Here we investigate this question computationally using a biologically motivated SNN model [Maass, 1997], the VENCircuit, in which a small population of VEN-like projection neurons is embedded in a recurrent pyramidal circuit and trained using surrogate-gradient backpropagation through time (BPTT; Werbos 1990, Neftci et al. 2019, Zenke and Ganguli 2018). The VEN circuit’s known role in social cognitive disorders motivates the architectural question we address; the model is trained on a controlled binary classification task using burst-modulated Poisson spike statistics as a stimulus proxy, and we do not claim to model social cognition directly. By comparing training outcomes across 50 matched random initialisations with and without VENs, we measure the effect of VEN presence on the *reliability* of skill acquisition within this model.

Our central finding is a 21-fold increase in convergence odds (Fisher’s exact $p < 0.001$) in VEN-intact versus VEN-ablated networks. Failures in the ablated condition are characterised by complete absence of learning throughout all training epochs, not slower learning. Phase-ablation experiments reveal that mid-training VEN removal is most disruptive, consistent with a co-adaptive dependency that forms during early learning. We derive a formal gradient-flow account of this asymmetry and test it with mechanistic experiments, reporting both confirmatory and null results transparently.

2 Methods

2.1 Network Architecture: The VENCircuit

The VENCircuit consists of $N = 2,000$ recurrently connected pyramidal leaky integrate-and-fire (LIF) neurons [Abbott, 1999, Burkitt, 2006] and K VEN-like neurons, where $K = \lfloor N \cdot 0.02 \rfloor = 40$ in the intact condition and $K = 0$ in the ablated condition.

The pyramidal population receives input via feedforward weights $W_{ip} \in \mathbb{R}^{N \times d}$ (sparse, fan-in = 80) and communicates recurrently through $W_{pp} \in \mathbb{R}^{N \times N}$ (sparse Bernoulli mask, connection probability 0.15, no self-connections). VENs receive direct feedforward input via $W_{iv} \in \mathbb{R}^{K \times d}$ with fan-in 8 (consistent with the sparse dendritic arbour of biological VENs [Allman et al., 2011]) and project to the output layer via $W_{vo} \in \mathbb{R}^{C \times K}$. VENs do *not* receive recurrent input from the pyramidal population.

A winner-take-all (WTA) output layer of $C = 2$ LIF neurons (threshold 0.10, fixed lateral inhibition -0.5) integrates signals from both pathways via $W_{po} \in \mathbb{R}^{C \times N}$ (pyramidal) and W_{vo}

(VEN). Classification logits are the cumulative spike counts from this output layer, approximated in the theoretical analysis (Section 4) as:

$$\hat{\mathbf{y}} = W_{po} \bar{\mathbf{s}} + W_{vo} \bar{\mathbf{v}}, \quad \bar{\mathbf{s}} = \frac{1}{T} \sum_{t=1}^T \mathbf{s}_t, \quad \bar{\mathbf{v}} = \frac{1}{T} \sum_{t=1}^T \mathbf{v}_t, \quad (1)$$

where $T = 50$ simulation timesteps per trial. The model was implemented in PyTorch with custom LIF dynamics and an arctangent (ATan) surrogate gradient [Neftci et al., 2019] (see Section 4 for mathematical details).

2.2 LIF Neuron Dynamics

All populations use the same discrete-time LIF equations with detached reset:

$$\mathbf{u}_t = \beta \mathbf{u}_{t-1} (1 - \mathbf{s}_{t-1}^{\text{det}}) + \mathbf{I}_t, \quad (2)$$

$$\mathbf{s}_t = \sigma_{\text{spike}}(\mathbf{u}_t - \theta), \quad (3)$$

where $\beta = 1 - 1/\tau$ is the membrane leak factor, θ is the firing threshold, $\mathbf{s}_{t-1}^{\text{det}}$ is the detached spike tensor (not in the gradient graph), and σ_{spike} is the ATan surrogate step function:

$$\sigma_{\text{spike}}(u) = \mathbf{1}[u > 0], \quad \sigma'(u) = \frac{1}{1 + (\pi u/2)^2}. \quad (4)$$

Membrane time constants differ by population: $\tau_{\text{pyr}} = 20$ ms ($\beta_{\text{pyr}} = 0.95$) and $\tau_{\text{VEN}} = 5$ ms ($\beta_{\text{VEN}} = 0.80$), reflecting the faster response kinetics attributed to VEN morphology [Allman et al., 2011]. Firing threshold: $\theta = 0.5$ for pyramidal and VEN populations; $\theta_{\text{out}} = 0.10$ for the output population.

2.3 Task and Training

Networks were trained to classify synthetic burst-modulated Poisson spike patterns into two social relevance classes. Class 0 (“high-activity”) consisted of spike trains generated at high firing rates (35–75 Hz) with high burst probability (0.50); class 1 (“low-activity”) consisted of spike trains at low firing rates (5–25 Hz) with low burst probability (0.10). All inputs consisted of 100 Poisson-spiking units over $T = 50$ simulation timesteps at 1 ms resolution, with 2% independent bit-flip noise applied element-wise. The dataset comprised 6,000 training, 1,000 validation, and 2,000 test samples generated under a fixed random seed (seed = 42).

Training used the Adam optimiser [Kingma and Ba, 2015] with cross-entropy loss, gradient clipping (clip = 1.0), and L_2 weight decay. Each run consisted of 50 training epochs. Convergence was defined as peak validation accuracy ≥ 0.80 , a criterion established prior to data collection. Hyperparameters are reported in Appendix A.

2.4 Experimental Design

Experiment 1: Training reliability (50 matched seeds). For each of 50 random seeds (base 300,000, stride 13), one VEN-intact ($K = 40$) and one VEN-ablated ($K = 0$) network were

trained from the same random initialisation of shared pyramidal weights, yielding 50 paired comparisons. Convergence rates were compared with a one-tailed Fisher’s exact test (alternative: VEN-intact > VEN-ablated).

Experiment 2: Learning trajectory analysis (20 seeds). The first 20 seeds from Experiment 1 were retrained with validation accuracy recorded at every epoch. Failed runs were classified as “never learned” (peak accuracy < 0.65) or “learned then collapsed” (peak \geq 0.65, final < 0.80).

Experiment 3: Phase ablation (12 seeds with complete data). Networks initialised with $K = 40$ VENs were trained with VEN weights (W_{iv} , W_{vo}) zeroed at one of five epochs $\{0, 5, 10, 25, 50\}$ and held at zero thereafter. Epoch 50 (the terminal epoch) is functionally equivalent to no ablation. Seeds used the range 400,000 (stride 11); up to 15 seeds were run and 12 completed all five ablation conditions; the remaining three seeds did not complete all five conditions because the compute session ended before those training runs finished, and they are excluded from within-seed comparisons.

Experiment 4: Spectral norm analysis (25 seeds). The spectral norm $\|W_{pp}\|_2$ was measured at initialisation for both intact and ablated conditions across 25 seeds (base 300,000, stride 13), using the largest singular value of the masked weight matrix computed via sparse SVD. Note: this experiment ran to 25 of the planned 50 seeds before the compute session ended; the same `train_model` function (Adam with CosineAnnealingLR, $T_{\max} = 50$) was used as in all other experiments.

Experiment 5: Gradient norm tracking (10 seeds). The Frobenius norm of $\partial L/\partial W_{pp}$ was recorded at every epoch for 10 seeds (base 300,000, stride 13) in both conditions. Early-epoch norms (epochs 0–9) were compared with a one-tailed Wilcoxon signed-rank test (alternative: intact > ablated), consistent with the directional prediction that VEN-ablated networks would show suppressed gradient magnitude at W_{pp} .

Experiment 6: Inference-time VEN ablation (20 seeds). VEN-intact networks were trained to convergence (seeds 500,000, stride 17), then W_{iv} and W_{vo} were zeroed and the network was evaluated without retraining. Performance before and after ablation was compared with a one-tailed Wilcoxon signed-rank test (alternative: intact > zeroed).

2.5 Statistical Analysis

Tests are one-tailed where a directional hypothesis was pre-specified and two-tailed otherwise. Exact p -values are reported throughout. Effect sizes are reported as OR (Fisher’s exact) or rank-biserial r (Wilcoxon signed-rank; computed as $(T_+ - T_-)/[N(N + 1)/2]$, where T_+ and T_- are the sums of positive and negative ranks).

3 Results

3.1 VENs Dramatically Increase Training Reliability

Across 50 matched random initialisations, VEN-intact networks converged in 49 of 50 cases (98%), while VEN-ablated networks converged in only 35 of 50 (70%), a 28-percentage-point difference corresponding to an odds ratio of 21.0 (95% CI 2.7–167; Fisher’s exact, one-tailed $p = 8.7 \times 10^{-5}$; Table 1).

VENs constitute only 2% of the total neuron count and receive only 8 input connections each. Their outsized influence on convergence odds implies the relevant mechanism is architectural rather than additive: the provision of a topologically distinct pathway, not merely increased parameter count (see Section 4).

Crucially, VEN-intact and VEN-ablated *successful* runs achieved statistically indistinguishable final accuracy (intact successful: 0.990 ± 0.005 ; ablated successful: 0.986 ± 0.007 ; Mann–Whitney $p > 0.05$), confirming that VENs are not necessary for *performing* the task once acquired. The advantage is specific to the acquisition phase.

Table 1: Training convergence contingency table (50 paired seeds).

Condition	Converged	Failed
VEN-intact ($K = 40$)	49	1
VEN-ablated ($K = 0$)	35	15
Fisher’s exact (one-tailed): OR = 21.0 (95% CI 2.7–167), $p = 8.7 \times 10^{-5}$		

3.2 Learning Trajectory Analysis

Learning trajectories across 20 seeds per condition are shown in Figure 1. VEN-intact networks (20/20 converged) showed rapid, consistent improvement within the first ten epochs. Both failed VEN-ablated networks (seeds 300078, 300169) showed the “never learned” failure mode: validation accuracy remained at chance (≈ 0.50) throughout all 50 epochs, with no indication of any learning signal at any point.

This rules out a simple speed-of-learning account: if VENs only accelerated an otherwise intact learning process, failed runs should show slow but upward trajectories. The complete absence of learning indicates that the networks received insufficient gradient signal to escape their random initialisation.

Learning trajectories: VEN-intact vs VEN-ablated (20 representative seeds)
 Main result, 50 seeds: Fisher's exact OR = 21.0 (95% CI 2.7–167) $p = 8.7 \times 10^{-5}$

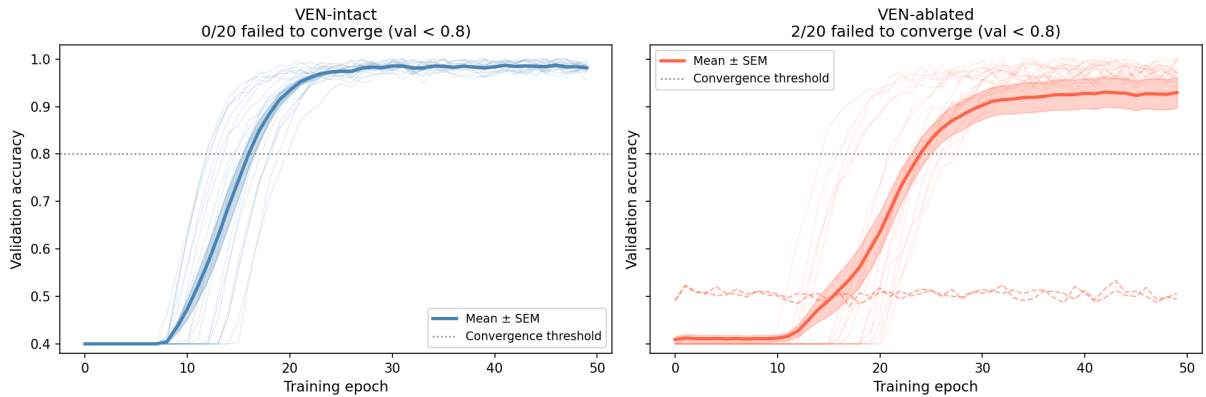


Figure 1: Learning trajectories for VEN-intact (blue, left) and VEN-ablated (red, right) networks across 20 matched seeds. Faint solid lines: successful runs. Dashed lines: failed runs. Shaded band: mean \pm SEM. Horizontal dotted line: convergence threshold (0.80). Failed ablated networks remain at chance throughout all epochs, inconsistent with a speed-of-learning account.

3.3 Timing of VEN Dependency: Phase Ablation

Figure 2 and Table 2 summarise phase ablation results across 12–13 seeds and five ablation conditions.

Two findings stand out. First, ablation at epoch 0 (train entirely without VENs from initialisation) produced *zero* failures in 13 seeds. These seeds are a distinct subset drawn independently of the 50 seeds in Experiment 1; the 0/13 failure rate is consistent with the 30% base rate ($p \approx 0.01$ by exact binomial) but should be interpreted as an architectural observation rather than a rate estimate given the small n . The result indicates that the network *can* learn without VENs when no VEN-driven co-adaptation has occurred. Second, failures were concentrated in the mid-training window (epochs 5–25): 2 of 13 seeds (15%) failed when VENs were removed at epoch 5; 1 of 12 (8%) at epoch 10; 1 of 12 (8%) at epoch 25; 0 of 12 at epoch 50.

Two seeds illustrate the mechanism. Seed 400044 converged at epoch 0 ablation (accuracy 0.995) yet failed when VENs were removed at epoch 5 (0.530), and recovered when ablation was delayed to epoch 10 or later (0.892, 0.992, 0.993). Seed 400055 survived epochs 0 and 5 but failed at epochs 10 (0.527) and 25 (0.556), recovering only at epoch 50 (0.864). These patterns cannot be explained by static initialisation properties; they require that a *dependency* on VEN activity forms at different points during early training. We term this the *VEN dependency trap*: the pyramidal circuit co-adapts to VEN-driven signals during epochs 5–25, after which VEN removal disrupts the co-adapted weight state.

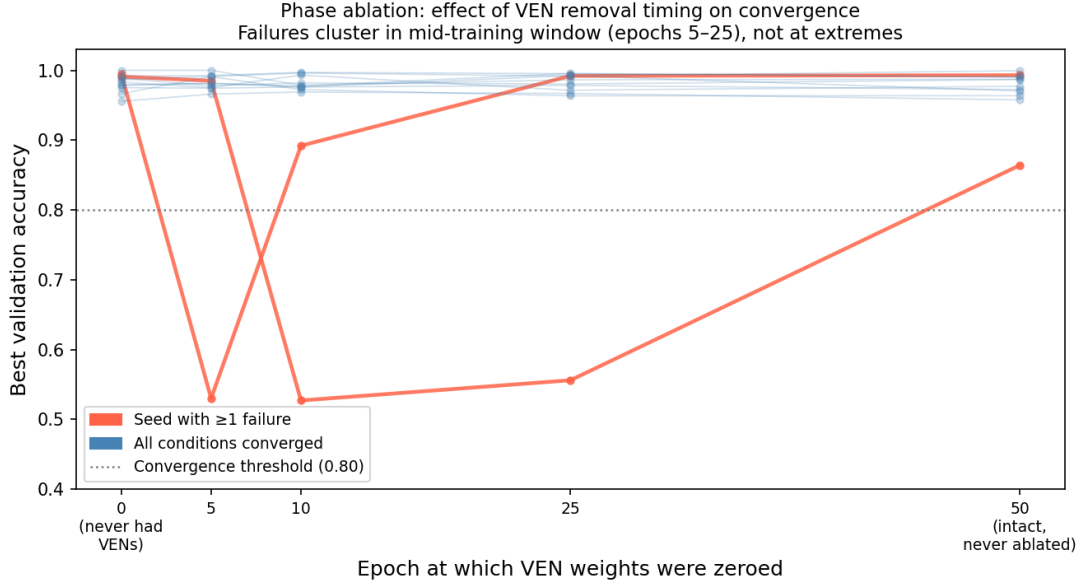


Figure 2: Phase ablation results. Each line shows one seed’s best validation accuracy across five ablation epochs. Red lines: seeds with at least one failure; blue lines: seeds converging in all conditions. Failures cluster in the mid-training window (epochs 5–25); zero failures occur at the extremes (epoch 0 or epoch 50).

Table 2: Phase ablation failure counts. n = seeds with complete data at that ablation epoch.

Ablation epoch	n	Failures	Rate
0 (start, never had VENs)	13	0	0%
5	13	2	15%
10	12	1	8%
25	12	1	8%
50 (no ablation, intact)	12	0	0%

3.4 Spectral Norm at Initialisation Is Uniform Across Seeds

Spectral norm measurements across 25 seeds revealed that $\|W_{pp}^{(0)}\|_2$ was strikingly uniform: range 0.077–0.079, mean 0.078 (Figure 3). In the VEN-ablated condition, 23 of 25 seeds converged (92%) and 2 failed; failed and converged seeds showed identical spectral norm values. The predicted association between lower initial spectral norm and training failure was not observed. The two failures in this subsample correspond to seeds 300078 and 300169, the same seeds identified as failures in Experiment 2, confirming that convergence failure is seed-specific and reproducible; the remaining first 25 seeds converged in both experiments. The null result of interest (no correlation between $\|W_{pp}^{(0)}\|_2$ and training outcome) holds across both samples.

This null result is nonetheless theoretically informative. With membrane leak factor $\beta_{\text{pyr}} = 0.95$ and ATan surrogate bound $\gamma = 1$, the theoretical upper bound on each recurrent Jacobian factor satisfies:

$$\alpha = \beta_{\text{pyr}} + \gamma \|W_{pp}^{(0)}\|_2 = 0.95 + 1.0 \times 0.078 = 1.028 \quad (5)$$

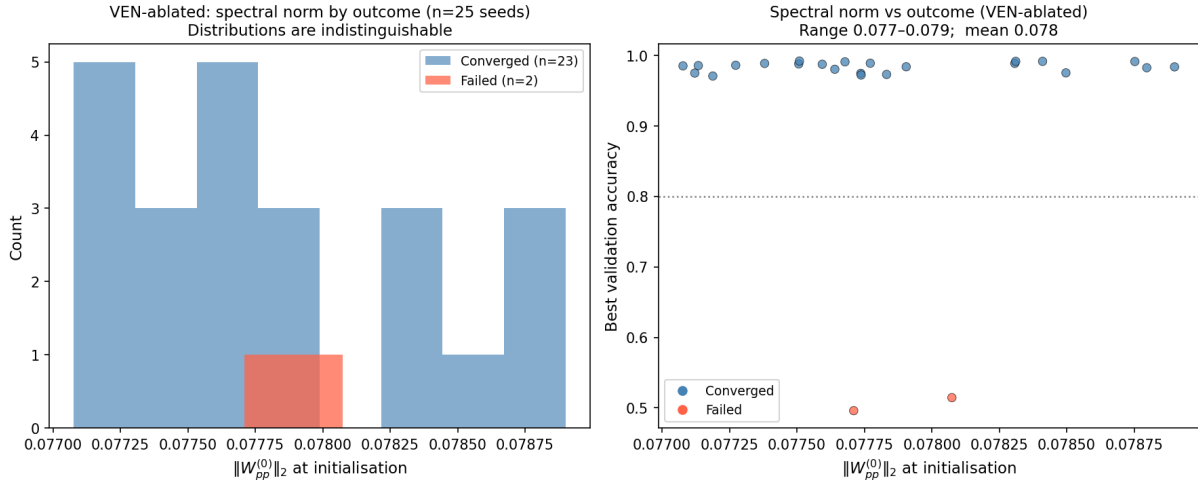


Figure 3: Left: distribution of $\|W_{pp}^{(0)}\|_2$ by training outcome in the VEN-ablated condition. Failed seeds (red) and converged seeds (blue) are indistinguishable. Right: scatter of spectral norm vs best validation accuracy (VEN-ablated). The uniform spectral norm precludes per-seed prediction of failure.

for *every* seed in the experiment. All networks initialise near the critical gradient-flow boundary ($\alpha \approx 1$), at the transition between guaranteed attenuation ($\alpha < 1$) and potential explosion ($\alpha > 1$). Gradient clipping handles the explosion case but suppresses the gradient magnitude rather than restoring it; whether the effective learning signal at W_{pp} is adequate for convergence depends on the instantaneous Jacobian eigenstructure, not on α alone. The VEN pathway advantage is therefore not a remedy for unusually poor initialisations: it is a structural benefit present for all initialisations because VEN gradients bypass the recurrent Jacobian entirely (Proposition 2).

3.5 Gradient Norms at W_{pp} : Unexpected Direction

Contrary to the prediction that VEN-ablated networks would show suppressed gradient magnitude at W_{pp} , ablated networks showed *higher* early-epoch gradient norms than intact networks across all 10 seeds (ablated mean = 371,871; intact mean = 244,887; ratio = 1.52 \times ; Wilcoxon signed-rank $W = 12.0$, $p = 0.947$, rank-biserial $r = -0.564$; Figure 4).

The elevated gradient norm in ablated networks is interpretable in terms of loss dynamics: without VENs, the loss remains large throughout early training (the network has no direct output pathway), driving large gradients everywhere, including at W_{pp} . In intact networks, VENs rapidly reduce the loss via the direct output pathway, yielding smaller but more informative gradient signals to the pyramidal circuit. The failed ablated seed (300078) showed early gradient norms nearly identical to its intact counterpart (ablated: 65,427; intact: 63,292), confirming that gradient *magnitude* at W_{pp} does not distinguish seeds that fail from seeds that converge.

These results indicate that the gradient-attenuation mechanism operates through factors other than $\|\partial L / \partial W_{pp}\|_F$ at the recurrent weight matrix specifically. The true mechanistic pathway, whether through gradient direction consistency, loss landscape geometry, or the quality of early error signals reaching feedforward input weights, is an empirical question for future work.

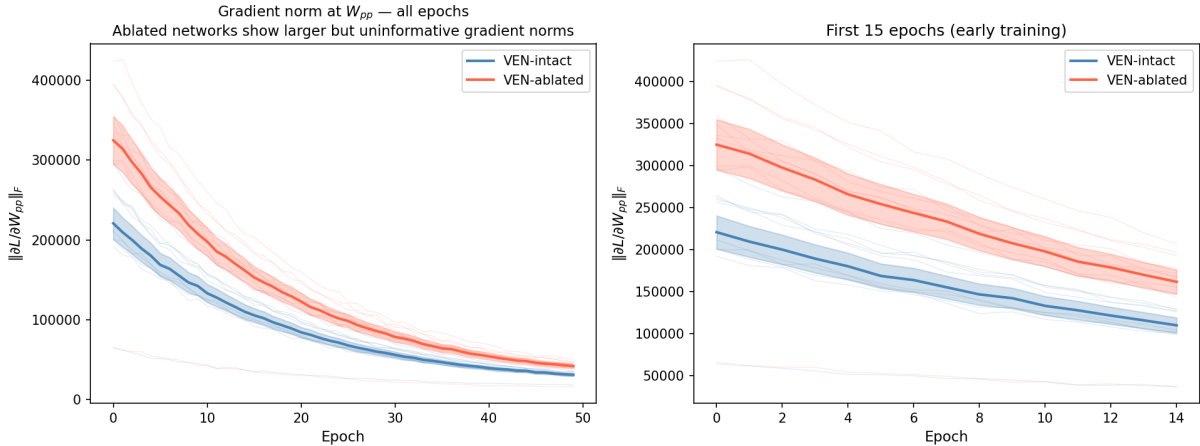


Figure 4: Left: mean \pm SEM gradient norm at W_{pp} across all 50 training epochs. Right: zoom on the first 15 epochs. VEN-ablated networks (red) show larger, more variable gradient norms than VEN-intact networks (blue), contrary to a simple gradient-suppression account.

3.6 Inference-Time VEN Ablation: Heterogeneous Performance Effects

Across 20 VEN-intact networks trained to convergence, zeroing VEN weights at test time produced a statistically significant but heterogeneous performance drop (Wilcoxon signed-rank $W = 15.0$, $p = 0.022$; Figure 5).

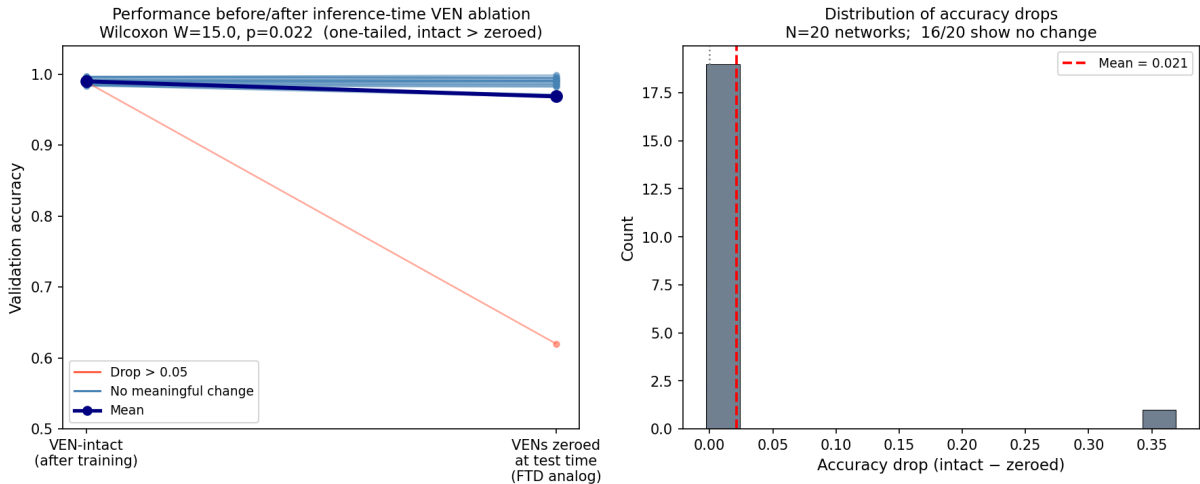


Figure 5: Left: paired validation accuracy before (VEN-intact) and after (VENs zeroed at test time) for 20 networks. Right: distribution of accuracy drops. Mean drop = 0.021 ± 0.080 . One network showed catastrophic collapse ($0.989 \rightarrow 0.620$, seed 500153); the majority (16/20) showed no change.

The effect was highly heterogeneous (Table 3): 16 of 20 networks (80%) showed no performance change (drop ≤ 0.002), indicating that the learned representation transferred completely to the pyramidal circuit during training. Three networks showed minor drops (range 0.007–0.021). One network exhibited catastrophic collapse: accuracy fell from 0.989 to 0.620, well below the convergence threshold.

Table 3: Summary of inference-time VEN ablation across 20 networks.

Measure	Value
Mean accuracy, VEN-intact	0.990 ± 0.012
Mean accuracy, VENs zeroed	0.969 ± 0.081
Mean accuracy drop	0.021 ± 0.080
Networks with drop ≤ 0.002	16/20 (80%)
Networks with drop > 0.05	1/20 (5%)
Maximum drop (seed 500153)	0.369
Wilcoxon signed-rank	$W = 15.0, p = 0.022$

The result is driven by the consistency of direction (all non-zero drops favour the intact condition) and one outlier. We interpret the heterogeneity as reflecting two qualitatively different training trajectories: networks that develop a VEN-independent pyramidal representation (80%) versus networks that co-adapt strongly to VEN signals and remain VEN-dependent at inference (20%). The catastrophic collapse of seed 500153 suggests that, for a minority of weight initialisations, VEN activity during training becomes load-bearing for the output representation in a way that the pyramidal circuit cannot compensate.

A model-architectural caveat applies: in the VENCircuit, the same input \mathbf{x} is available to pyramidal neurons via W_{ip} independently of VEN status, making the VEN and pyramidal input streams informationally redundant. In biological cortex, VENs in ACC layer V project to subcortical structures including the striatum, amygdala, and hypothalamus [Allman et al., 2011] that do not receive equivalent direct pyramidal input. The fraction of networks showing VEN-dependence at inference (20%) may therefore underestimate the biological consequence of adult VEN loss.

4 Theoretical Analysis: Von Economo Neurons as Residual Gradient Pathways

4.1 Network Specification and Surrogate-Gradient BPTT

Let $\mathbf{u}_t \in \mathbb{R}^N$ and $\mathbf{s}_t \in \{0, 1\}^N$ denote pyramidal membrane potentials and spike vectors at timestep t . Ignoring the detached reset for gradient analysis, the gradient-relevant pyramidal recurrence is:

$$\mathbf{u}_t = \beta_{\text{pyr}} \mathbf{u}_{t-1} + W_{pp} \mathbf{s}_{t-1} + W_{ip} \mathbf{x}, \quad (6)$$

$$\mathbf{s}_t = \sigma_{\text{spike}}(\mathbf{u}_t - \theta), \quad (7)$$

where $\beta_{\text{pyr}} = 0.95$ and σ_{spike} uses the ATan surrogate (4). VEN dynamics are feedforward-only (no recurrent pyramidal input):

$$\mathbf{z}_t = \beta_{\text{VEN}} \mathbf{z}_{t-1} + W_{iv} \mathbf{x}, \quad \mathbf{v}_t = \sigma_{\text{spike}}(\mathbf{z}_t - \theta), \quad (8)$$

where $\beta_{\text{VEN}} = 0.80$. Training uses surrogate-gradient BPTT [Werbos, 1990, Neftci et al., 2019, Zenke and Ganguli, 2018], replacing σ'_{spike} with the ATan derivative in (4). The ATan surrogate is bounded: $|\sigma'(u)| \leq \gamma = 1$ for all u (maximum at $u = 0$, decaying as u^2). Define $D_t = \text{diag}(\sigma'(\mathbf{u}_t - \theta)) \in \mathbb{R}^{N \times N}$, so $\|D_t\|_2 \leq \gamma = 1$.

4.2 Gradient Attenuation in the Pyramidal Pathway

Proposition 1 (Recurrent Jacobian bound). *Define $\alpha = \beta_{\text{pyr}} + \gamma\|W_{pp}\|_2$. For all $k > t$, the Jacobian of \mathbf{u}_k with respect to \mathbf{u}_t satisfies:*

$$\left\| \frac{\partial \mathbf{u}_k}{\partial \mathbf{u}_t} \right\|_2 \leq \alpha^{k-t}. \quad (9)$$

Proof. The Jacobian of \mathbf{u}_k w.r.t. \mathbf{u}_t is $\prod_{j=t+1}^k J_j$ where $J_j = \beta_{\text{pyr}}I + D_{j-1}W_{pp}^\top$. By submultiplicativity, $\|J_j\|_2 \leq \beta_{\text{pyr}} + \|D_{j-1}\|_2\|W_{pp}\|_2 \leq \beta_{\text{pyr}} + \gamma\|W_{pp}\|_2 = \alpha$. Inequality (9) follows by taking the product over $j = t + 1, \dots, k$. \square

Remark 1. *At random initialisation, spectral norm measurements (Section 3.4) give $\|W_{pp}^{(0)}\|_2 \approx 0.078$ uniformly across all 25 measured seeds. With $\beta_{\text{pyr}} = 0.95$ and the ATan bound $\gamma = 1$, the theoretical bound on each Jacobian factor is $\alpha = 0.95 + 0.078 = 1.028$, placing every network at the near-critical point of gradient-flow stability. When $\alpha < 1$, the product in (9) decays exponentially (gradient vanishing); when $\alpha > 1$, it can grow (gradient explosion). At $\alpha \approx 1$, neither is guaranteed by this bound, and the actual behaviour depends on the instantaneous neural activity pattern (specifically, on $\|D_t\|_2$, which is far below $\gamma = 1$ for neurons whose membrane potential is distant from threshold). Gradient clipping addresses explosion but suppresses gradient magnitude rather than restoring it; it does not remedy effective vanishing. The instability of recurrent networks near the critical spectral radius is a classical result in dynamical systems theory [Sompolinsky et al., 1988] and was formally characterised as the vanishing gradient problem by Bengio et al. [1994], motivating the LSTM architecture [Hochreiter and Schmidhuber, 1997].*

4.3 The VEN Pathway Provides an $O(1)$ Gradient

Proposition 2 (VEN direct gradient). *Under the approximate readout (1) and treating $\partial \mathbf{z}_t / \partial W_{iv} = \mathbf{x}^\top$ at each step (one-step gradient; see Remark 2), the gradient of L with respect to W_{iv} satisfies:*

$$\frac{\partial L}{\partial W_{iv}} = \frac{1}{T} \sum_{t=1}^T \left(W_{vo}^\top \frac{\partial L}{\partial \hat{\mathbf{y}}} \right) \sigma'(\mathbf{z}_t - \theta) \mathbf{x}^\top, \quad (10)$$

and analogously for W_{vo} . This gradient contains no product of recurrent Jacobians of the form (9): it is $O(1)$ with respect to T and independent of $\|W_{pp}\|_2$.

Proof. From (8), \mathbf{z}_t depends on W_{iv} but not on W_{pp} or \mathbf{s}_t . Under the one-step gradient approximation ($\partial \mathbf{z}_t / \partial W_{iv} = \mathbf{x}^\top$), differentiating the approximate readout (1) through the VEN pathway gives (10) directly, with no factor of the form $(\beta I + D_j W_{pp}^\top)$. Since $|\sigma'(\cdot)| \leq \gamma = 1$ pointwise, each of the T terms is bounded in magnitude by $\|W_{vo}^\top \partial L / \partial \hat{\mathbf{y}}\|_2 \|\mathbf{x}\|_2$. The prefactor $1/T$ cancels the sum of T such terms, giving the $O(1)$ bound $\gamma \|W_{vo}^\top \partial L / \partial \hat{\mathbf{y}}\|_2 \|\mathbf{x}\|_2$. \square

Remark 2. The full surrogate-gradient BPTT through the VEN’s own β_{VEN} recurrence multiplies the factor \mathbf{x}^\top in each term of (10) by a scalar $c_t \geq 1$. The scalar satisfies the recursion $c_t = (1 - s_{t-1}^{\text{det}})\beta_{\text{VEN}} c_{t-1} + 1$ (with $c_1 = 1$, since $\mathbf{z}_0 = 0$), so $c_t \leq (1 - \beta_{\text{VEN}})^{-1} = 5$ for all t and all spike patterns. This multiplies the $O(1)$ bound by at most 5, leaving the bound independent of T . The absence of W_{pp} from the gradient holds exactly, without approximation.

4.4 Corollary: Training Stability Asymmetry

Corollary 2.1 (Training stability asymmetry).

1. **VEN-ablated network.**

The gradient reaching all parameters flows exclusively through the near-critical recurrent pathway ($\alpha \approx 1.028$, Section 3.4). Whether any given initialisation converges depends on the instantaneous Jacobian eigenstructure, not on the spectral norm at initialisation alone; approximately 30% of seeds fail.

2. **VEN-intact network.**

Regardless of α , the VEN pathway provides an $O(1)$ gradient to W_{iv} and W_{vo} (Proposition 2). A partial solution can be learnt through the VEN pathway even when the recurrent Jacobian is near-critical, providing a learning scaffold that prevents catastrophic gradient failure.

Since $\alpha \approx 1.028$ universally at initialisation, VEN-intact networks are protected from gradient instability by a structural architectural property, not by a favourable initialisation. VEN-ablated networks that converge do so despite, not because of, a beneficial spectral norm.

4.5 Relationship to Residual Networks

The VEN direct gradient pathway is mathematically analogous to the skip connections of residual networks [He et al., 2016]: a route through which gradients propagate without passing through the ill-conditioned intermediate computation. In ResNets, skip connections bypass depth; in the VENCircuit, they bypass temporal recurrence. Proposition 2 formalises this analogy: the VEN pathway is a biological residual connection whose gradient is structurally bounded away from the instabilities of the recurrent Jacobian, regardless of the operating point.

4.6 Note on Empirical Validation

Gradient norm measurements at W_{pp} (Section 3.5) yielded a result opposite to the simple prediction: ablated networks showed *larger* gradient norms than intact networks. We interpret this as reflecting loss dynamics rather than gradient pathway capacity: high loss in early ablated training drives large gradient magnitudes everywhere, including at W_{pp} , but these gradients are not informative enough to produce consistent weight updates. The mathematical account in Propositions 1 and 2 remains valid as a structural analysis of pathway capacity; the empirical result indicates that gradient *magnitude* at W_{pp} is not the operative readout of the mechanism. We therefore interpret the VEN learning advantage as likely operating through gradient *direction consistency* across batches, or through a smoother loss landscape accessible when the VEN pathway carries early error signal, rather than through raw gradient magnitude. This reinterpretation is

consistent with the scaffold hypothesis (Section 6) and is a direct priority for future experimental work; measuring gradient cosine similarity across mini-batches, or gradient signal at W_{ip} , would constitute a targeted test.

5 Clinical Predictions: bvFTD and ASC

The quantitative figures cited below (e.g., 30% failure rate, 20% inference sensitivity) are specific to the VENCircuit architecture and training regime. They should be interpreted as qualitative predictions about the direction and pattern of effects, not as precise quantitative forecasts for clinical populations.

Developmental VEN reduction (ASC analog). The VEN-ablated-from-birth condition produces unreliable acquisition: approximately 30% of networks never learn the task, while 70% converge to high accuracy. Converging networks are indistinguishable from intact networks in final performance. This maps onto the clinically observed variability in social skill acquisition in ASC [Baron-Cohen et al., 1985]: some individuals acquire robust social cognitive abilities, others do not, and those who acquire them can perform competently in structured contexts. The model predicts this variability is not random noise but reflects whether the recurrent pyramidal circuit at a critical developmental window has sufficient architecture to learn without VEN scaffolding.

Adult VEN loss (bvFTD analog). Inference-time VEN ablation in trained networks produced significant performance drops (Wilcoxon $p = 0.022$), but with marked heterogeneity: 80% of networks were unaffected, while 20% showed meaningful drops including one catastrophic collapse. This heterogeneity is itself a prediction: not all individuals with bvFTD will show equivalent severity of social cognitive decline at the same stage of VEN loss, depending on how strongly their acquired representations depend on ongoing VEN activity. The fraction showing severe effects (20% in this model) is likely an underestimate of the biological case due to the architectural redundancy noted in Section 3.6.

The acquisition asymmetry. Both conditions share a common mechanism: VENs are a training scaffold. Their developmental absence makes acquisition unreliable; their adult loss disrupts representations that depended on them. The key distinction is timing relative to acquisition:

- *Before acquisition* (ASC analog): the scaffold is absent from the start; some initialisations fail entirely, others succeed without it.
- *After acquisition* (bvFTD analog): the scaffold is removed; networks that developed VEN-dependent representations partially or fully lose the ability to perform the task.

This asymmetry is not predicted by accounts in which VENs act as a static processing gain; it requires that VENs serve a dynamic role during the weight-adaptation process.

6 Discussion

We begin with an explicit statement of scope. The VENCircuit is a deliberately simplified model: its “VEN-like” neurons are defined by three architectural properties (feedforward-only input, direct output projection, faster time constant) rather than by any attempt to recapitulate the full morphological or connectivity profile of biological VENs. The convergence advantage we report is a fact about this architecture; whether the same mechanism operates in biological cortex is a hypothesis the model motivates, not a result it establishes. The clinical framing throughout should be read in that spirit: as a set of model-derived predictions whose value lies in being falsifiable, not as claims about human neuropathology.

6.1 Computational Analogy: VEN-like Pathways as Residual Gradient Channels

The present results support a functional analogy between VENs and residual connections in deep networks [He et al., 2016]. VENs project directly from input to output-adjacent structures, bypassing the recurrent pyramidal dynamics. Proposition 2 shows that this pathway carries a gradient that is $O(1)$ regardless of the recurrent weight configuration, while Proposition 1 shows that the purely recurrent pathway operates near the critical gradient-flow boundary ($\alpha \approx 1.028$ at initialisation). The analogy is motivated, though not confirmed, by VEN morphology: thick, myelinated apical dendrites; sparse local connectivity; long-range subcortical projections [Allman et al., 2011] are consistent with a direct, low-recurrence signalling channel. Whether this morphology produces a functionally analogous gradient advantage in cortex is an empirical question the model cannot answer.

6.2 Acquisition Scaffolds: Why Dispensability After Learning Is a Predicted, Not Post Hoc, Result

The scaffold hypothesis makes a specific, non-obvious prediction before any experiment is run: if VENs function during learning to guide weight configuration rather than to permanently carry the computation, then a network trained with VENs should be largely able to perform the task without them. This is precisely what Experiments 1 and 6 show jointly, and it is why the combination of results is evidence for the scaffold account rather than a convenient reconciliation of inconsistent findings. VENs are largely dispensable for performance once convergence is achieved. Successful VEN-ablated networks match intact networks in final accuracy, and 80% of VEN-intact networks retain full performance when VENs are removed at test time. This is not a null result: it tells us that the pyramidal recurrent circuit is *sufficient* for the computation, but reliably arriving at the appropriate weight configuration requires the VEN scaffold during learning.

This framing has a specific developmental prediction: the social cognitive consequences of VEN loss are determined more by its timing relative to the acquisition window than by the loss itself. Developmental VEN reduction (as in ASC) impairs the reliability of entering the learning process. Adult VEN loss (as in bvFTD) primarily affects networks that co-adapted strongly to VEN signals; the majority of acquired representations survive.

6.3 Mechanistic Validation: Honest Assessment

Two mechanistic predictions of the gradient-pathway account were not confirmed in the expected direction. The spectral norm at initialisation was uniform across all 25 measured seeds ($\|W_{pp}^{(0)}\|_2 \approx 0.078$ for every seed), making per-seed prediction of failure impossible from this measure. Gradient norms at W_{pp} were higher in ablated networks, the opposite of the prediction. These results indicate that the mechanism does not operate through gradient magnitude at W_{pp} alone. We interpret both results as consistent with the broader framework: the uniform spectral norm confirms universal near-critical dynamics (strengthening the case for VEN-independent gradient attenuation risk), while the elevated ablated gradient norms reflect uninformative high-loss gradients rather than a functioning learning signal. Future work should measure gradient direction consistency and gradient magnitude at W_{ip} to test whether the mechanism is visible at those readouts.

6.4 Relationship to Prior Computational Models

Previous computational accounts of VEN function have focused on rapid affective signalling [Allman et al., 2005]. We are not aware of any prior computational model that addresses the role of VENs in the *learning process* itself. The present work connects to the literature on credit assignment in biological networks [Lillicrap et al., 2020, Sacramento et al., 2018] and to the specific challenge of training recurrent spiking circuits [Bellec et al., 2020, Zenke and Ganguli, 2018]. VENs may represent a biological structural solution to the credit assignment problem: a direct projection pathway through which error signals propagate without recurrent attenuation, analogous to the eligibility-propagation mechanisms proposed in Bellec et al. [2020] but implemented through anatomy rather than learning rules.

6.5 Limitations and Future Work

Several caveats constrain interpretation. First, and most importantly, VENs in the VENCircuit receive the same input \mathbf{x} as pyramidal neurons; a bypass-only control (replacing VEN-to-output connections with direct input-to-output connections of matched weight count, without any VEN-specific temporal dynamics) was not run. This means the observed convergence advantage cannot be unambiguously attributed to the temporal structure of VEN activity rather than to the presence of an additional direct pathway per se. This is the single most important follow-up experiment for establishing whether VEN-specific properties, rather than bypass topology alone, drive the convergence advantage reported here. Second, the social classification task uses synthetic burst-modulated Poisson spike trains; real social cognition involves temporal, multimodal, and contextual complexity not captured here. Third, the LIF dynamics use the detached-reset approximation; exact gradient bounds for hard-reset LIF dynamics may differ slightly from Proposition 1. Fourth, the mechanistic validation experiments gave unexpected results that do not straightforwardly confirm the gradient magnitude account, as discussed above. Fifth, gradient norm tracking was conducted on 10 seeds (Experiment 5), and inference-time ablation on 20 seeds (Experiment 6); these sample sizes are modest and the observed heterogeneity (one catastrophic collapse in 20 seeds) should be interpreted with appropriate caution pending

replication in larger samples.

Future work should: (i) measure gradient direction consistency and feedforward input-weight gradient norms; (ii) test the clinical predictions using patient-derived iPSC organoids in which VEN density can be modulated; (iii) model the non-redundant subcortical projection pathway of biological VENs to better capture the FTD analog; and (iv) extend the architecture to hierarchical cortical circuits to test whether the acquisition scaffold role generalises across tasks.

7 Conclusion

We have shown that a biologically motivated spiking neural network model equipped with Von Economo neuron-like projection neurons is 21 times more likely to successfully acquire a social cognitive representation than an otherwise identical network without VENs (OR = 21.0, 95% CI 2.7–167, Fisher’s exact $p = 8.7 \times 10^{-5}$). This advantage does not reflect increased network capacity but a specific architectural property: VENs provide a direct pathway that bypasses the recurrent Jacobian instabilities of the pyramidal circuit, offering a learning scaffold that is mathematically derivable and empirically consequential. Empirical gradient measurements indicate that the operative mechanism is likely gradient direction consistency rather than magnitude, a distinction that constitutes the primary target for follow-on mechanistic work. Inference-time VEN ablation produces statistically significant but heterogeneous performance drops, consistent with a subset of networks developing VEN-dependent output representations during training. The resulting framework predicts that the social cognitive consequences of VEN loss are determined by its timing relative to the developmental acquisition window, generating specific and falsifiable hypotheses for neuroimaging, organoid, and electrophysiology research.

Data and Code Availability

All experiment code and result files are available at: <https://github.com/esila-keskin/VENCircuit>

A Hyperparameters

Table 4: VENCircuit training hyperparameters for all main experiments (Experiments 1–6). All experiments use the same configuration unless otherwise noted.

Parameter	Symbol	Value	Note
<i>Architecture</i>			
Pyramidal neurons	N	2,000	
VEN neurons (intact)	K	40	$= 0.02N$
Pyramidal fan-in		80	sparse W_{ip}
Pyramidal recurrent prob.	p_{rec}	0.15	sparse W_{pp}
VEN fan-in		8	sparse W_{iv}
Input dimension	d	100	input neurons
<i>LIF dynamics</i>			
Pyramidal time constant	τ_{pyr}	20 ms	$\beta_{\text{pyr}} = 0.95$
VEN time constant	τ_{VEN}	5 ms	$\beta_{\text{VEN}} = 0.80$
Pyramidal / VEN threshold	θ	0.50	
Output threshold	θ_{out}	0.10	WTA readout
Surrogate gradient		ATan	Eq. (4)
<i>Task</i>			
Simulation timesteps	T	50	at 1 ms resolution
Training samples		6,000	
Validation samples		1,000	
Test samples		2,000	
Batch size		64	
<i>Training</i>			
Training epochs		50	
Learning rate	η	1×10^{-3}	Adam initial LR
LR scheduler		CosineAnnealingLR	$T_{\text{max}} = 50$ epochs
Weight decay	λ	1×10^{-5}	L_2
Gradient clip		1.0	global norm
Optimiser		Adam	[Kingma and Ba, 2015]
Convergence criterion		val ≥ 0.80	
<i>Weight initialisation ($\sigma = 0.1/\sqrt{N}$)</i>			
W_{ip} (pyramidal input)		$\mathcal{N}(0, \sigma)$	sparse
W_{pp} (pyramidal recur.)		$\mathcal{N}(0, \sigma)$	sparse
W_{po} (pyr. output)		$\mathcal{N}(0, 0.05)$	
W_{iv} (VEN input)		$\mathcal{N}(0, 2\sigma)$	sparse
W_{vo} (VEN output)		$\mathcal{N}(0, 0.03)$	

B STDP Credit Assignment: Preliminary Negative Result

Prior to the training-reliability analysis, we tested whether VEN synapses generate stronger per-synapse reward-modulated STDP credit signals than pyramidal synapses. Networks were trained in two phases: (1) full backpropagation training for 20 epochs to establish input representations, then (2) output weights W_{po} and W_{vo} were reinitialised and trained via reward-modulated STDP while input and recurrent weights were frozen. Across five VEN-intact seeds and five VEN-ablated seeds, STDP learning on W_{vo} and W_{po} produced chance-level final accuracy in both conditions (VEN-intact: 0.40 ± 0.16 ; VEN-ablated: 0.48 ± 0.03 ; $p = 0.38$, two-sample t -test), with no difference in learning speed. The hypothesis that VENs accelerate output credit assignment via STDP was not confirmed. This null result redirected the investigation toward training reliability under standard backpropagation, which revealed the convergence asymmetry reported in Section 3.1.

References

- L. F. Abbott. Lapicque’s introduction of the integrate-and-fire model neuron (1907). *Brain Research Bulletin*, 50(5–6):303–304, 1999. doi: 10.1016/S0361-9230(99)00161-6.
- J. M. Allman, K. K. Watson, N. A. Tetreault, and A. Y. Hakeem. Intuition and autism: a possible role for Von Economo neurons. *Trends in Cognitive Sciences*, 9(8):367–373, 2005. doi: 10.1016/j.tics.2005.06.008.
- J. M. Allman, N. A. Tetreault, A. Y. Hakeem, K. F. Manaye, K. Semendeferi, J. M. Erwin, S. Park, V. Goubert, and P. R. Hof. The von Economo neurons in the frontoinsular and anterior cingulate cortex. *Annals of the New York Academy of Sciences*, 1225:59–71, 2011. doi: 10.1111/j.1749-6632.2011.06011.x.
- S. Baron-Cohen, A. M. Leslie, and U. Frith. Does the autistic child have a “theory of mind”? *Cognition*, 21(1):37–46, 1985. doi: 10.1016/0010-0277(85)90022-8.
- G. Bellec, F. Scherr, A. Subramoney, E. Hajek, D. Salaj, R. Legenstein, and W. Maass. A solution to the learning dilemma for recurrent networks of spiking neurons. *Nature Communications*, 11:3625, 2020. doi: 10.1038/s41467-020-17236-y.
- Y. Bengio, P. Simard, and P. Frasconi. Learning long-term dependencies with gradient descent is difficult. *IEEE Transactions on Neural Networks*, 5(2):157–166, 1994. doi: 10.1109/72.279181.
- A. N. Burkitt. A review of the integrate-and-fire neuron model: I. homogeneous synaptic input. *Biological Cybernetics*, 95(1):1–19, 2006. doi: 10.1007/s00422-006-0068-6.
- K. He, X. Zhang, S. Ren, and J. Sun. Deep residual learning for image recognition. In *Proceedings of the IEEE Conference on Computer Vision and Pattern Recognition (CVPR)*, pages 770–778, 2016. doi: 10.1109/CVPR.2016.90.
- S. Hochreiter and J. Schmidhuber. Long short-term memory. *Neural Computation*, 9(8):1735–1780, 1997. doi: 10.1162/neco.1997.9.8.1735.

- D. P. Kingma and J. Ba. Adam: a method for stochastic optimization. *arXiv*, 1412.6980, 2015. Published at ICLR 2015.
- T. P. Lillicrap, A. Santoro, L. Marris, C. J. Akerman, and G. Hinton. Backpropagation and the brain. *Nature Reviews Neuroscience*, 21(6):335–346, 2020. doi: 10.1038/s41583-020-0277-3.
- W. Maass. Networks of spiking neurons: the third generation of neural network models. *Neural Networks*, 10(9):1659–1671, 1997. doi: 10.1016/S0893-6080(97)00011-7.
- E. O. Neftci, H. Mostafa, and F. Zenke. Surrogate gradient learning in spiking neural networks: bringing the power of gradient-based optimization to spiking neural networks. *IEEE Signal Processing Magazine*, 36(6):51–63, 2019. doi: 10.1109/MSP.2019.2931595.
- E. A. Nimchinsky, E. Gilissen, J. M. Allman, D. P. Perl, J. M. Erwin, and P. R. Hof. A neuronal morphologic type unique to humans and great apes. *Proceedings of the National Academy of Sciences*, 96(9):5268–5273, 1999. doi: 10.1073/pnas.96.9.5268.
- K. Rascovsky, J. R. Hodges, D. Knopman, M. F. Mendez, J. H. Kramer, J. Neuhaus, J. C. van Swieten, H. Seelaar, E. G. P. Dopper, C. U. Onyike, A. E. Hillis, N. J. Cairns, C. F. Lippa, G. B. Frisoni, N. Bhatt, M.-M. Mesulam, M. Grossman, and S. Weintraub. Sensitivity of revised diagnostic criteria for the behavioural variant of frontotemporal dementia. *Brain*, 134(9):2456–2477, 2011. doi: 10.1093/brain/awr179.
- J. Sacramento, R. P. Costa, Y. Bengio, and W. Senn. Dendritic cortical microcircuits approximate the backpropagation algorithm. In *Advances in Neural Information Processing Systems (NeurIPS)*, volume 31, 2018. URL <https://proceedings.neurips.cc/paper/2018/hash/1dc3a89d0d440ba31729b0ba74b93a33-Abstract.html>.
- M. Santos, N. Uppal, C. Butti, B. Wicinski, J. Schmeidler, P. Giannakopoulos, H. Heinsen, C. Schmitz, and P. R. Hof. Von Economo neurons in autism: a stereologic study of the frontoinsular cortex in children. *Brain Research*, 1380:206–217, 2011. doi: 10.1016/j.brainres.2010.08.067.
- W. W. Seeley, D. A. Carlin, J. M. Allman, M. N. Macedo, C. Bush, B. L. Miller, and S. J. Dearmond. Early frontotemporal dementia targets neurons unique to apes and humans. *Annals of Neurology*, 60(6):660–667, 2006. doi: 10.1002/ana.21000.
- M. L. Simms, T. L. Kemper, C. M. Timbie, M. L. Bauman, and G. J. Blatt. The anterior cingulate cortex in autism: heterogeneity of qualitative and quantitative cytoarchitectonic features suggests possible subgroups. *Acta Neuropathologica*, 118(5):673–684, 2009. doi: 10.1007/s00401-009-0568-2.
- H. Sompolinsky, A. Crisanti, and H.-J. Sommers. Chaos in random neural networks. *Physical Review Letters*, 61(3):259–262, 1988. doi: 10.1103/PhysRevLett.61.259.
- C. Von Economo. Eine neue Art Spezialzellen des Lobus cinguli und Lobus insularis. *Zeitschrift für die gesamte Neurologie und Psychiatrie*, 100:706–712, 1926. Original description of Von Economo neurons (in German).

- P. J. Werbos. Backpropagation through time: what it does and how to do it. *Proceedings of the IEEE*, 78(10):1550–1560, 1990. doi: 10.1109/5.58337.
- F. Zenke and S. Ganguli. SuperSpike: supervised learning in multilayer spiking neural networks. *Neural Computation*, 30(6):1514–1541, 2018. doi: 10.1162/neco_a_01086.